Int. J. Heat Mass Transfer. Vol. 17, pp. 1191–1207. Pergamon Press 1974. Printed in Great Britain

THE SOLUTION OF A TWO-DIMENSIONAL FREEZING PROBLEM INCLUDING CONVECTION EFFECTS IN THE LIQUID REGION

P. G. KROEGER*
Casting Laboratory, Chase Brass and Copper Company, Cleveland, Ohio

and

S. OSTRACH
Case Western Reserve University, Cleveland, Ohio, U.S.A.

(*Received* 2 *October* 1973)

Abstract—To simulate a continuous casting process the temperature and flow field during solidification of a pure metal in a moving slab is considered. The analysis includes natural convection effects in the liquid pool.

Strong natural convection flows occur at Grashof numbers of 10^5–10^6. However, for the range of parameters investigated the natural convection had a negligible effect on the solid–liquid interface position.

Various qualitative aspects of the combined forced and natural convection flow field in the liquid pool are presented. Even for very strong natural convection the effect of the flow field on the temperature field remains relatively minor, its predominant tendency is to enhance the formation of an almost isothermal region at the bottom of the pool.

NOMENCLATURE

c, specific heat;
g, gravitational body force component in X-direction;
Gr, Grashof numbers, $Gr = \dfrac{g\beta(T_f - T_s)Y_0^3}{\nu^2}$;
h_i, scale factor of curvilinear coordinate system;
k, thermal conductivity;
n, number of node points in the quarter-circle;
$\mathbf{n}$, unit vector normal to the interface, pointing into the solid region;
N, number of node points in the half-circle;
p_d, nondimensional dynamic pressure;
P, Peclet number of the solid;
(P), Cauchy principal value of an integral;
P_d, dynamic pressure;
Pr, Prandtl number;
q, angular node spacing;
r, radial polar coordinate;
Re, Reynolds number;
S, Stefan number, nondimensional latent heat, $S = \dfrac{\Delta H}{c_S(T_s - T_0)}$;
S^*, ambient Stefan number, equation (78);
T, temperature;
T, transformation matrix;
T_f, feed metal temperature;
T_0, slab outside surface temperature;
u, coordinate of (u, v) plane;
u, nondimensional velocity component in x-direction, $u = \dfrac{U - U_w}{U_0}$;
U, X-component of velocity;
U, radius ratio function in conformal mapping;
U_f, feed velocity;
U_w, withdrawal velocity;
U_0, characteristic velocity;
v, coordinate of (u, v) plane;
v, nondimensional velocity component in y-direction, $v = \dfrac{V}{U_0}$;
V, Y-component of velocity;
V, angular distortion function in conformal mapping;
$\mathbf{V}$, velocity vector;
w, complex variable of (u, v) plane;
W_n, interface velocity normal to interface;
x, nondimensional vertical coordinate, $x = X/Y_0$;
x_p, nondimensional liquid region pool depth;

*Present address: Transportation Technology Center, General Electric Co., Erie, Pennsylvania 16501, U.S.A.

X, vertical coordinate;
X_p, liquid region pool depth;
y, nondimensional horizontal coordinate, $y = Y/Y_0$;
$\hat{y}(x)$, nondimensional solid–liquid interface position;
Y, horizontal coordinate;
Y_0, characteristic dimension in Y-direction, half width of slab;
$\hat{Y}(X)$, solid–liquid interface position;
z, complex variable of the physical (x, y) plane;
α, thermal diffusivity;
β, volumetric expansion coefficient, defined by (A16);
ΔH, latent heat;
ζ, complex variable of the mapped (ξ, η) plane;
η, coordinate in (ξ, η) plane;
θ, nondimensional solid region temperature;
Θ, nondimensional liquid region temperature;
Θ, angular polar coordinate;
μ, conductivity–temperature ratio;
μ, coordinate in (v, μ) plane;
ν, kinematic viscosity;
ν, coordinate in (v, μ) plane;
ξ, coordinate in (ξ, η) plane;
ρ, density;
ρ, radial polar coordinate;
σ, radial polar coordinate in (v, μ) plane following general conformal mapping;
τ, nondimensional temperature scale, equation (75);
ϕ, angular polar coordinate;
Φ, combined natural and forced convection stream function;
χ, complex variable of (v, μ) plane;
Ψ, angular polar coordinate in (v, μ) plane following general conformal mapping;
ψ, nondimensional stream function, defined by (36) describing natural convection flow field;
Ω, vorticity, defined by (39).

Subscripts

amb, ambient;
c, cooling;
L, liquid region;
s, at solidification temperature;
S, solid region;
SH, superheat;
0, reference variable in nondimensionalization.

Superscripts

i, iteration index;
j, iteration index.

1. INTRODUCTION

HEAT transfer with freezing or melting is of considerable importance, for instance during the casting of metals, in various chemical processes, as ablation during space craft re-entry, in icing of heat exchangers and wind tunnels, and also in various geological problems. Due to the release or absorption of latent heat during the change of phase such problems are generally nonlinear and substantially more difficult to solve than the corresponding single-phase problems.

In this work the freezing front position, the temperature field and the liquid region flow field will be analyzed for the specific case of a continuous casting process using a pure metal or a eutectic alloy, solidifying along a plane freezing front.

A typical continuous casting process is shown in Fig. 1: liquid metal, usually 50–100°K above solidification temperature is supplied continuously at the top of a bottomless mold. In the mold, the molten metal is cooled indirectly, for instance, by circulating cooling water through passages in the mold walls. Due to this heat removal from the molten metal a solid skin is formed. If some of the core is still liquid at the bottom of the mold, the strength of the solidified skin must be sufficient to contain the remaining liquid and permit continuous withdrawal of the casting.

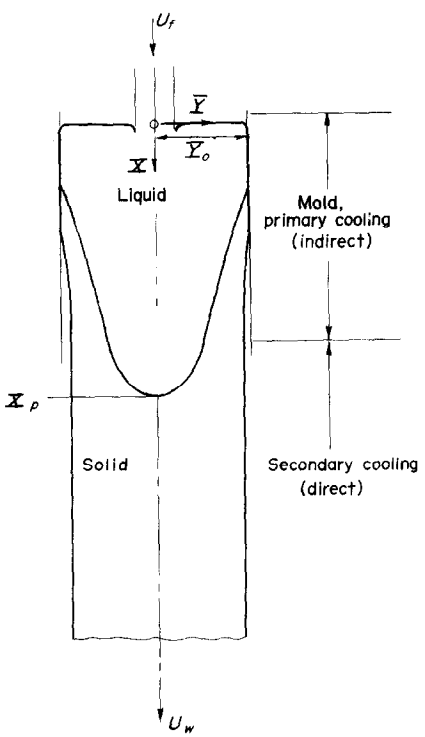

FIG. 1. Schematic diagram of a continuous casting process.

Below the mold, in the secondary cooling zone, water sprays are usually applied directly onto the casting surface.

For the configuration of Fig. 1 a forced flow field different from the slug flow of the solid will result if the feed metal is being supplied through a feed hole of smaller cross section than the casting. As the metal is supplied with superheat at the top of the liquid region and is cooled from the sides, a natural convection field must be expected in addition to the forced flow field.

Previous work has almost exclusively concentrated on the temperature field and freezing front position, assuming the liquid to move in slug flow, with no motion relative to the solid region. The effect of the flow field on the freezing front position will be shown here to be generally small. However, in industrial casting processes the flow field has a significant effect on the solidification process itself and on the ultimate cast structure. Therefore, it is of great interest to have a good understanding of the flow field in the liquid region and its driving forces. Accordingly it is highly desirable to include convection effects in such analyses.

2. PREVIOUS WORK

Analytical closed form solutions of the pure conduction problem with solidification have only been obtained for very few extremely idealized situations. For example, the temperature field in a one-dimensional semi-infinite medium and with a boundary condition of the first kind at the outside surface (i.e. constant surface temperature) constitutes the famous Stefan problem, with its solution by Neumann [1]. For finite bodies and for less restrictive boundary conditions various approximate methods have been applied after introducing further simplifying assumptions, such as neglecting the thermal capacitance in the solid region [2], as assuming the liquid to be initially at the freezing temperature, i.e. neglecting superheat [3–6].

For solutions in finite bodies, with superheat in the liquid, and in particular for multi-dimensional problems, numerical finite-difference or finite-element methods appear to offer the most practical approach [7–10]. These contributions can be classified into two major groups.

(1) The single-region methods apply the energy equation once over the complete domain, covering both phases. The latent heat release is simulated by appropriate modification of the specific heat or enthalpy.

(2) The multiple-region methods apply the energy equation separately for each phase and specify the proper coupling boundary conditions between the phases.

In general, the single-region approach leads to simpler models while the multiple-region approach offers more accurate solutions. Dusinberre [7] and Eyres *et al.* [8] for instance used the single region model in early work. Murray and Landis [9] developed two double-region methods for one dimensional freezing problems and demonstrated the increased accuracy of such models over the single-region methods. In the first of their models a fixed number of nodes is distributed uniformly in each phase and the size of each node varies as the one phase grows and the other phase disappears. In the second method the nodes are of equal size, fixed in space, and the finite difference equations at the node points next to the interface are adjusted to account for the interface travel between the node points.

The second method has recently been extended to multi-dimensional transient freezing problems by Lazaridis [10].

Almost all investigations considering the temperature field during solidification in continuous casting processes have assumed slug flow in the liquid. Hills [11] and Veynik [12] have applied approximate models, using an integral method, and neglecting superheat as well as axial conduction. Their solutions are much easier to use than the typical finite difference solutions, and they are valuable tools for the analysis of some continuous casting processes. However, their simplifying assumptions introduce inaccuracies, primarily in shallow pools, as well as in the bottom region of deep pools [13].

Models including axial conduction and superheat in the feed metal have only been solved by numerical methods, using the single region approach. Klein [14] and Adenis, Coats and Ragone [15] presented models for the solidification of alloys. Kroeger [13] handled the case of a pure metal.

The effect of convection in the liquid pool of a continuous casting process has hardly received any attention until very recently. The first contribution appears to be by Szekely and Stanek [16]. They consider potential flow between the feed metal orifice and the liquidus front, and slug flow in the mushy and solid regions of a continuous casting process for alloys. Viscous effects and natural convection effects are not included. Their numerical solution of the energy equation also neglects axial conduction effects. Relative to a model assuming slug flow in the liquid, their results show a marked effect of the flow field on the liquid temperature field and on the liquidus front, but almost no effect on the solidus front. The implications of this result are important: Several models described above [11–15] have solved the energy equation assuming slug flow in the liquid. Szekely and Stanek's more general model of potential flow in the liquid

showed no significant effect on the solidus front, i.e. on the point of final solidification and on the domain of the solid. Thus, the previous models which disregarded details of the flow field in the liquid region will be sufficient to predict the solidus front position and the solid region temperature field, as required for process design and productivity studies. However, the width of the mushy zone and the liquid temperature field have a significant effect on the solidification process and on the ultimate cast structure. Thus, consideration of liquid region effects is important in studies directed towards improving our understanding of the effects of the flow and temperature field on the solidification process and on the ultimate cast structure.

3. PROBLEM SELECTION

While Szekely and Stanek [16] considered some of the forced flow effects it is intended to concentrate here on the contribution of natural convection due to cooling from the sides, superimposed over a uniform forced flow field. The ratio Gr/Re^2 of Grashof and Reynolds number for typical casting processes ranges from about 1–10 and significant natural convection flows can therefore be expected.

Considerations shall be confined here to plane front solidification of a pure metal, where the change of phase occurs at one distinct solid–liquid interface and at a constant temperature T_s. For alloys the fluid velocities relative to the solid in the mushy region, are generally several orders smaller than those of the liquid region [17]. Significant concentration gradients are in general also restricted to the mushy region, except, maybe, at the dendrite tips, But for liquid metals the Schmidt number $Sc = \nu/D$ is of the order of 100, and, therefore, even at the dendrite tips concentration gradients will occur only over distances small with respect to those for velocity and temperature gradients. Thus, the selected model of the flow field during solidification of a pure metal should also provide a first approximation for the liquid region flow field in many commercial alloys of practical interest.

The feed flow at $X = 0$ will be assumed laminar, with uniform feed velocity over the complete cross section $\mathbf{V} = (U_f, 0)$ and with constant feed temperature $T_f > T_s$ (see Fig. 1).

The geometry of a two-dimensional slab casting will be selected with no changes normal to the X–Y plane. Cooling of the casting outside surface will be modeled by a constant temperature boundary condition $T = T_0 < T_s$. In this case freezing will always begin at the feed level, $X = 0$.

For this idealized process, the temperature and flow field in the liquid, the solid temperature field, and the freezing front position during steady state operation are of interest. The interface position, of course, depends on the temperature and flow fields and must be determined as part of the solution. A general method of solving this free surface problem will be developed here, and some qualitative aspects of the combined forced and natural convection effects will be presented. The restriction to qualitative results is dictated not only by the above idealization of the process, but also by our present inability to impose accurate boundary conditions for mold and spray cooling. Further, in many cases our knowledge of several of the key material properties is insufficient to permit accurate quantitative predictions.

4. THE MATHEMATICAL MODEL

A solution of the natural convection field in the liquid requires a knowledge of the interface position, which determines the domain of the liquid. For accurate results a two region model is preferrable, i.e. the governing equations are applied separately to the liquid and to the solid domain, with the appropriate boundary conditions for the field variables and one additional boundary condition for the interface position. The liquid region equations for a quasi incompressible Newtonian fluid with constant material properties* are

$$\frac{\partial U}{\partial X} + \frac{\partial V}{\partial Y} = 0 \tag{1}$$

$$U\frac{\partial U}{\partial X} + V\frac{\partial U}{\partial Y} = -\beta g(T - T_s) - \frac{1}{\rho_s}\frac{\partial P_d}{\partial X} + \nu\left(\frac{\partial^2 U}{\partial X^2} + \frac{\partial^2 U}{\partial Y^2}\right) \tag{2}$$

$$U\frac{\partial V}{\partial X} + V\frac{\partial V}{\partial Y} = -\frac{1}{\rho_s}\frac{\partial P_d}{\partial Y} + \nu\left(\frac{\partial^2 V}{\partial X^2} + \frac{\partial^2 V}{\partial Y^2}\right) \tag{3}$$

$$U\frac{\partial T}{\partial X} + V\frac{\partial T}{\partial Y} = \alpha_L\left(\frac{\partial^2 T}{\partial X^2} + \frac{\partial^2 T}{\partial Y^2}\right). \tag{4}$$

The liquid region boundary conditions follow with the above idealizations of constant feed flow velocity and temperature as

$$X = 0; 0 < Y < Y_0: \quad U = U_f; V = 0; T = T_f \tag{5}$$

$$0 < X < X_p; Y = 0: \quad \frac{\partial U}{\partial Y} = 0; V = 0; \frac{\partial T}{\partial Y} = 0. \tag{6}$$

At the interface, assuming no discontinuity in density there is:

$$Y = \hat{Y}(X): \quad U = U_w; V = 0; T = T_s \tag{7}$$

*For a more detailed justification of these assumptions, see [18].

For the solid region, assuming the material properties to be constant, but not necessarily the same as in the liquid, the energy equation is

$$U_w \frac{\partial T}{\partial X} = \alpha_S \left(\frac{\partial^2 T}{\partial X^2} + \frac{\partial^2 T}{\partial Y^2} \right). \tag{8}$$

The boundary conditions for the solid region include equation (7) and with the above idealization of constant casting surface temperature

$$0 < X < \infty ; Y = Y_0 : \quad T = T_0 \tag{9}$$

$$X_p < X < \infty ; Y = 0 : \quad \frac{\partial T}{\partial Y} = 0 \tag{10}$$

$$X \to \infty ; 0 < Y < Y_0 : \quad T = T_0 . \tag{11}$$

The coupling boundary condition for the free surface is obtained from conservation of energy across the interface:

$$-k_S \frac{\partial T_S}{\partial n} + k_L \frac{\partial T_L}{\partial n} = \rho_s \Delta H . \mathbf{V}_S . \mathbf{n}. \tag{12}$$

Considering thermal boundary-layer thicknesses for free convection along a vertical plate in a semi-infinite liquid metal [19] one finds that except in very wide castings a thermal boundary layer which begins its growth at $X = 0$ along the solid–liquid interface $Y = \hat{Y}(X)$ would soon exceed the casting width. The liquid region temperature field can, therefore, not be treated as a boundary-layer problem, and the full elliptic equation must be solved without further simplifications. Viscous effects, however, remain restricted to a relatively small layer close to the boundary.

In combined forced and free convection flow of liquid metals significant peak velocities beyond the slug flow field can occur at the interface [20] for the Gr/Re^2 values of typical casting processes ($\approx 1{\cdot}5$–10). On the other hand, with the boundary conditions imposed by the interface, the horizontal temperature gradients and thus the bouyancy forces will decrease towards the bottom of the pool. Further, conservation of mass requires that any peak velocities created in the top regions of the pool must subside towards the bottom of the pool. One of the objectives of this work will be to assess whether as a result of these opposing effects significant velocity peaks can be expected in typical processes of interest. Thus, the flow field boundary conditions at the interface constitute an essential part of the problem, and they must be satisfied on all sides of the pool or cavity. This requires that the flow equations be solved in their elliptic form, without further simplifications. For these conditions the following relationships were selected to non-dimensionalize the above equations:

$$x = X/Y_0 ; \quad y = Y/Y_0 \tag{13}$$

$$u = \frac{U - U_w}{U_0} ; \quad V = \frac{V}{U_0} ; \quad p_d = \frac{P_d}{\rho_s U_0^2} \tag{14}$$

$$\Theta = \frac{T - T_s}{T_f - T_s} ; \quad \theta = \frac{T - T_0}{T_s - T_0} . \tag{15}$$

The choice of characteristic velocity U_0 remains to be made. One could choose the feed flow and withdrawal velocity U_w. However, since attention is primarily concentrated here on natural convection it may be more appropriate to select the U_0 based on these peak velocities.

It was found above that one should expect viscous effects to remain restricted to small regions close to the wall. Thus, over most of the fluid domain buoyancy and inertia effects will dominate, and for Gr/Re^2 somewhat larger but not orders larger than unity it appears that the characteristic velocity U_0 resulting from a balance of inertia and buoyancy terms would be advantageous [19]:

$$U_0 = \sqrt{(g\beta \Delta T Y_0)}. \tag{16}$$

With these relationships the non-dimensional governing equations are:
Liquid region:

$$\frac{\partial u}{\partial x} + \frac{\partial v}{\partial y} = 0 \tag{17}$$

$$\left(\frac{Re}{\sqrt{(Gr)}} + u \right) \frac{\partial u}{\partial x} + v \frac{\partial u}{\partial y} = -\Theta - \frac{\partial p_d}{\partial x} + \frac{1}{\sqrt{(Gr)}} \left(\frac{\partial^2 u}{\partial x^2} + \frac{\partial^2 u}{\partial y^2} \right) \tag{18}$$

$$\left(\frac{Re}{\sqrt{(Gr)}} + u \right) \frac{\partial v}{\partial x} + v \frac{\partial v}{\partial y} = -\frac{\partial p_d}{\partial y} + \frac{1}{\sqrt{(Gr)}} \left(\frac{\partial^2 v}{\partial x^2} + \frac{\partial^2 v}{\partial y^2} \right) \tag{19}$$

$$\left(\frac{Re}{\sqrt{(Gr)}} + u \right) \frac{\partial \Theta}{\partial x} + v \frac{\partial \Theta}{\partial y} = \frac{1}{Pr \sqrt{(Gr)}} \left(\frac{\partial^2 \Theta}{\partial x^2} + \frac{\partial^2 \Theta}{\partial y^2} \right) \tag{20}$$

with boundary conditions:

$$x = 0 ; 0 < y < 1{\cdot}0 : \quad u = v = 0 ; \Theta = 1{\cdot}0 \tag{21}$$

$$0 < x < x_p ; y = 0 : \quad \frac{\partial u}{\partial y} = 0 ; v = ; \frac{\partial \Theta}{\partial y} = 0 \tag{22}$$

$$y = \hat{y}(x) : \quad u = v = 0 ; \Theta = 0 \tag{23}$$

Solid region:

$$\frac{\partial \theta}{\partial x} = \frac{1}{P} \left(\frac{\partial^2 \theta}{\partial x^2} + \frac{\partial^2 \theta}{\partial y^2} \right) \tag{24}$$

with boundary conditions:

$$y = \hat{y}(x): \quad \theta = 1{\cdot}0 \tag{25}$$

$$0 < x < \infty; y = 1{\cdot}0: \quad \theta = 0 \tag{26}$$

$$x_p < x < \infty; y = 0: \quad \frac{\partial \theta}{\partial y} = 0 \tag{27}$$

$$x \to \infty; 0 < y < 1{\cdot}0: \quad \theta = 0. \tag{28}$$

In scaling the interface boundary condition it is advantageous to express the normal derivatives and the normal unit vector of equation (12) in terms of temperature gradients:

$$\frac{\partial T_i}{\partial n} = \nabla T_i . \mathbf{n}; i = S, L; \quad \mathbf{n} = -\frac{\nabla T_i}{|\nabla T_i|}; i = S, L. \tag{29}$$

One then obtains from (12):

$$k_S \frac{\nabla T_S . \nabla T_S}{|\nabla T_S|} - k_L \frac{\nabla T_L . \nabla T_L}{|\nabla T_S|} = -\rho_s \Delta H \frac{\mathbf{V}_S . \nabla T_S}{|\nabla T_S|}. \tag{30}$$

Since the liquid and solid temperature gradients have the same direction at the interface, and since $\mathbf{V}$ has no component in the Y-direction the above equation can be simplified to

$$k_S |\nabla T_X| - k_L |\nabla T_L| = -\rho_s \Delta H \, U_w \frac{\partial T_S / \partial X}{|\nabla T_S|} \tag{31}$$

which becomes in non-dimensional form

$$|\nabla \theta| - \mu |\nabla \Theta| = -PS \frac{\partial \theta / \partial x}{|\nabla \theta|} \tag{32}$$

or

$$-\frac{\partial \theta}{\partial n} + \mu \frac{\partial \Theta}{\partial n} = PS \, n_x \tag{33}$$

where S is the Stefan number, or non-dimensional latent heat:

$$S = \frac{\Delta H}{c_S (T_s - T_0)} \tag{34}$$

and μ a conductivity–temperature ratio:

$$\mu = \frac{k_L (T_f - T_s)}{k_S (T_s - T_0)}. \tag{35}$$

To assess the order of the various terms of (32) it is convenient to write it as

$$|\nabla \theta| \left(1 - \mu \left| \frac{\nabla \Theta}{\nabla \theta} \right| \right) = -PS \frac{\partial \theta / \partial x}{|\nabla \theta|}. \tag{32a}$$

This equation expresses that the latent heat release due to freezing of metal passing through the interface (right side) equals the heat flux out of the interface into the solid minus the heat flux from the liquid into the interface (left side). The second term in the left side parentheses represents the ratio of heat flux from the liquid into the solid. Integrated over the complete interface this represents the ratio of superheat to latent heat plus superheat, i.e.

$$\frac{c_L (T_f - T_s)}{\Delta H + c_L (T_f - T_s)}.$$

For typical feed metal temperatures of 50–100°K above T_s the ratio is 0·085–0·17 for pure copper. Similar values apply for other metals. For this reason the average effect of the liquid temperature field on the gross interface position is minor.

If the overall effect of the liquid temperature gradient on the interface equation is small, then the effect of convection on the interface position, which enters only through the effect of convection on the liquid temperature gradient, will be even smaller. This is in agreement with Szekelly and Stanek's observation [16] of negligible effect of convection on the solidus front position in the freezing of alloys. In the top regions of deep pools $n_x = \partial \theta / \partial x / |\nabla \theta|$ can be small, and thus, the right side of equation (32a) can be small. The magnitude of the liquid side heat flux then approaches that of the solid side. However, such deep pools which are common in the steel industry will not be considered here. For solution of the above equations it is advantageous to transform the liquid region equations into the stream function/vorticity form. Introducing

$$u = \frac{\partial \psi}{\partial y}; \quad v = -\frac{\partial \psi}{\partial x} \tag{36}$$

and

$$\Omega = \frac{\partial v}{\partial x} - \frac{\partial u}{\partial y} = -\nabla^2 \psi \tag{37}$$

the continuity equation (17) is satisfied identically and two momentum equations (18) and (19) reduce to

$$\left(\frac{Re}{\sqrt{(Gr)}} + \frac{\partial \psi}{\partial y} \right) \frac{\partial \Omega}{\partial x} - \frac{\partial \psi}{\partial x} \frac{\partial \Omega}{\partial y} = \frac{\partial \Theta}{\partial y} + \frac{1}{\sqrt{(Gr)}} \nabla^2 \Omega. \tag{38}$$

$$\nabla^2 \psi = -\Omega.$$

The energy equation now becomes:

$$\left(\frac{Re}{\sqrt{(Gr)}} + \frac{\partial \psi}{\partial y} \right) \frac{\partial \Theta}{\partial x} - \frac{\partial \psi}{\partial x} \frac{\partial \Theta}{y} = \frac{1}{Pr \sqrt{(Gr)}} \nabla^2 \Theta \tag{40}$$

while the boundary conditions can be expressed as

$$x = 0; 0 < y < 1{\cdot}0: \quad \psi = \frac{\partial \psi}{\partial x} = 0; \Theta = 1{\cdot}0 \tag{41}$$

$$0 < x < x_p; y = 0: \quad \psi = \frac{\partial^2 \psi}{\partial y^2} = 0; \frac{\partial \Theta}{\partial y} = 0 \tag{42}$$

$$y = \hat{y}(x): \quad \psi = \frac{\partial \psi}{\partial n} = 0; \Theta = 0. \tag{43}$$

5. METHOD OF SOLUTION

The problem is fully described by the liquid region governing equations and boundary conditions (38)–(43), the solid region equation and boundary conditions (24)–(28), plus the interface boundary condition (32). To solve this system of simultaneous equations for the field variables ψ, Ω, Θ and θ and for the interface position $y = \hat{y}(x)$ numerical finite-difference methods appear to be most practical. The solid as well as the liquid region have the boundary $y = \hat{y}(x)$ which in general does not fall onto a coordinate line. In such field problems a coordinate transformation such that all boundaries become coordinate lines is highly desirable, in particular if finite difference methods are used,* thus avoiding non-even and non-orthogonal nodal arrangements at the boundary. Of the great multitude of transformations that could be selected for this purpose a conformal transformation appeared to be most advantageous, since the othogonality of the coordinate system is retained, resulting in relatively simple transformed equations and single term boundary conditions. In particular mixed derivatives which can cause numerical stability problems are avoided.

However, the use of such a transform also adds to the complexity of the problem since it requires the solution of an additional subproblem, namely to find the conformal mapping. For a boundary of arbitrary shape this will usually require a numerical, iterative solution procedure. For the free-surface problem under consideration here, which must be solved iteratively, this mapping will even have to be recomputed during the iteration process. Nevertheless, it was felt that adding this numerical mapping problem was justified by the increased ease and accuracy of solving the governing equations in the mapped domain where all its boundaries are coordinate lines.

The general iterative solution procedure will then be as follows:

(1) Assume a temperature, stream function, and vorticity distribution in the liquid domain, and temperature distribution in the solid domain.

(2) Assume a solid–liquid interface position.

(3) Determine a conformal mapping between the solid domain and a transformed domain where all boundaries are coordinate lines; do the same for the liquid domain.

(4) Solve the transformed governing equations in the transformed plane.

(5) Transform the solution, and in particular the interface temperature gradients, into the physical plane.

(6) Obtain an improved interface position by satisfying the interface boundary condition with the temperature gradients from step 5.

(7) Repeat the iterative sequence beginning with step 3.

To employ this procedure the mapped domains for both solid and liquid regions must be selected and the conformal mappings between the physical domains and the mapped domains must be determined, including the transformation matrices. The essential points of the mapping procedure are summarized in Appendix A. Complete details are given in [18]. Both solid and liquid regions were separately mapped by a sequence of transformations into parts of the unit circle. Theodorsen's integral equation was applied to obtain the conformal mapping of the general interface $y = \hat{y}(x)$ into the unit circle. Wittich's method was used to solve the integral equation iteratively. This method as selected converged for the shallow pools of primary interest in this work. Modifications to be applied for deep pools are discussed briefly in Appendix A and in more detail in [18].

6. SOLUTION IN THE TRANSFORMED PLANE

The transformation of the governing equations from the physical plane to the mapped plane can readily be accomplished with the general transformation relationships between cartesian and orthogonal curvilinear coordinates [25]. With finite difference methods it has generally been advantageous to express the transport terms of the governing equations in the conservation form [26, 27]. Using $\nabla . \mathbf{v} = 0$ one obtains from (38)–(40) for right-handed curvilinear coordinates

$$\frac{1}{h_1 h_2}\left[\frac{\partial}{\partial \rho}\left(\frac{\partial y}{\partial \phi}\frac{Re}{\sqrt{(Gr)}}+\frac{\partial \psi}{\partial \phi}\right)\Omega-\frac{\partial}{\partial \phi}\left(\frac{\partial y}{\partial \rho}\frac{Re}{\sqrt{(Gr)}}+\frac{\partial \psi}{\partial \rho}\right)\Omega\right] = \frac{1}{h_1 h_2}\left(-\frac{\partial x}{\partial \phi}\frac{\partial \Theta}{\partial \rho}+\frac{\partial x}{\partial \rho}\frac{\partial \Theta}{\partial \phi}\right)+\frac{1}{\sqrt{(Gr)}}\nabla^2\Omega \quad (44)$$

$$\nabla^2\psi = -\Omega \quad (45)$$

and

$$\frac{1}{h_1 h_2}\left[\frac{\partial}{\partial \rho}\left(\frac{\partial y}{\partial \phi}\frac{Re}{\sqrt{(Gr)}}+\frac{\partial \psi}{\partial \phi}\right)\Theta-\frac{\partial \psi}{\partial \phi}\left(\frac{\partial y}{\partial \rho}\frac{Re}{\sqrt{(Gr)}}+\frac{\partial \psi}{\partial \rho}\right)\Theta\right] = \frac{1}{Pr\sqrt{(Gr)}}\nabla^2\Theta \quad (46)$$

with

$$\nabla^2 F = \frac{1}{h_1 h_2}\left[\frac{\partial}{\partial \rho}\left(\frac{h_2}{h_1}\frac{\partial F}{\partial \rho}\right)+\frac{\partial}{\partial \phi}\left(\frac{h_1}{h_2}\frac{\partial F}{\partial \phi}\right)\right]. \quad (47)$$

The boundary conditions for the liquid region become:

$$\phi = \frac{\pi}{2}; 0 < \rho < 1: \quad \psi = \frac{\partial \psi}{\partial \phi} = 0; \Theta = 1{\cdot}0 \quad (48)$$

$$\phi = 0; 0 < \rho < 1: \quad \psi = \frac{\partial^2 \psi}{\partial \phi^2} = 0; \frac{\partial \Theta}{\partial \phi} = 0 \quad (49)$$

$$0 < \phi < \frac{\pi}{2}; \rho = 1: \quad \psi = \frac{\partial \psi}{\partial \rho} = 0; \Theta = 0 \quad (50)$$

The solid governing equation in right-handed curvilinear coordinates follows from (24) in the same way:

$$\frac{1}{h_1 h_2}\left(\frac{\partial y}{\partial \phi}\frac{\partial \theta}{\partial \rho}-\frac{\partial y}{\partial \rho}\frac{\partial \theta}{\partial \phi}\right)=\frac{1}{P}\nabla^2\theta \tag{51}$$

with the boundary conditions:

$$\phi=\frac{\pi}{2};0<\rho<1:\quad \theta=0 \tag{52}$$

$$\phi=0;0<\rho<1:\quad \frac{\partial\theta}{\partial\phi}=0 \tag{53}$$

$$0<\phi<\frac{\pi}{2};\rho=1:\quad \phi=1{\cdot}0. \tag{54}$$

The above equations can readily be expressed in finite difference form using the general second order central difference formulas. Details are given in [18]. The use of centered difference formulas in the inertia and convection terms is preferable resulting in smaller truncation errors of the finite difference approximations. However in iterative solutions of this form stability considerations impose a limit to relatively small values of Gr, Re and Pr. For the low Prandtl numbers of liquid metals the restriction to small Reynolds and Grashof numbers in the vorticity equation is generally the limiting point. In the present work with 18×18 nodes no stability problems arose with Gr up to 10^6, and higher values have not been used. For $Re=100$ rapid divergence occurred in the vorticity equation while the method converged well at $Re=50$.

For the liquid region the resulting finite difference equations present a system of simultaneous nonlinear algebraic equations, three for each node point. For the solid region one obtains a set of simultaneous linear algebraic equations, one for each node point.

Numerical application of the stream function and temperature boundary conditions is straightforward. For the vorticity equations direct boundary conditions are not prescribed and one must apply (45) at the boundaries with (48)–(50) to obtain boundary conditions in terms of the vorticity. On $\phi=0$ one finds readily

$$\phi=0:\quad \Omega=0 \tag{55}$$

while on the other boundaries

$$\phi=\frac{\pi}{2}:\quad \Omega=-\frac{1}{h_2^2}\frac{\partial^2\psi}{\partial\phi^2} \tag{56}$$

and

$$\rho=1:\quad \Omega=-\frac{1}{h_1^2}\frac{\partial^2\psi}{\partial\rho^2}. \tag{57}$$

The latter two conditions together with $\partial\psi/\partial\phi=0$ on $\phi=\pi/2$ and $\partial\psi/\partial\rho=0$ on $\rho=1$ can be used with the proper finite difference formulas to express the boundary values of Ω in terms of the stream function in the vicinity of the boundary. Several approaches have been suggested by various workers, as summarized by Mallinson and de Vahl Davis [28]. Here the most common second order approximation has been used in resulting in the following equations for the vorticity on the boundaries $\phi=\pi/2$ and $\rho=1{\cdot}0$:

$$\phi=\frac{\pi}{2}:\quad \Omega_0=-\frac{1}{2h_2^2\Delta\phi^2}(8\psi_{-1}-\psi_{-2}) \tag{58}$$

and

$$\rho=1:\quad \Omega_0=-\frac{1}{2h_1^2\Delta\rho^2}(8\psi_{-1}-\psi_{-2}) \tag{59}$$

where the subscript 0 designates a node point on the boundary, while -1 and -2 refer to node points 1 or 2 node spacings removed from the boundary. The general iterative solution of the finite difference equations follows the outline of Section 5. During each overall iteration, i.e. for each interface position the simultaneous equations for the solid and liquid region must also be solved iteratively in inner loops. In the liquid region one uses during the ith iteration the stream function field of the $(i-1)$th iteration to compute the nonlinear transport terms. The energy and vorticity equations are then solved with these coefficients as a quasi-linear set of equations. Thereafter, the "new" vorticity values are used to compute the ith stream function field. The alternating direction method was used to solve the sets of simultaneous equations for both regions.

With the solution procedure of Section 5 the interface boundary condition must be satisfied in the physical plane. Thus, it does not have to be transformed itself, however, the temperature gradients along the unit circle in the mapped plane $\partial\Theta/\partial\rho$ and $\partial\theta/\partial\rho$ must be transformed into the corresponding interface temperature gradients in the physical plane using

$$\frac{\partial\theta}{\partial n}=-\frac{1}{h_{1_S}}\frac{\partial\theta}{\partial\rho};\quad \frac{\partial\Theta}{\partial n}=\frac{1}{h_{1_L}}\frac{\partial\Theta}{\partial\rho}. \tag{60}$$

For the iterative solution of the interface boundary condition it was found most convenient to consider the iteration procedure as a pseudo transient where the interface moves with velocity W_n normal to itself or by

$$\Delta s=W_n\Delta t \tag{61}$$

within the pseudo time interval Δt. From equation (33) the equation for this pseudo velocity follows with (60) as

$$W_n=U_w\left[n_x-\frac{1}{PS}\left(\frac{1}{h_{1_S}}\frac{\partial\theta}{\partial\rho}+\mu\frac{1}{h_{1_L}}\frac{\partial\Theta}{\partial\rho}\right)\right] \tag{62}$$

and the interface position of the jth iteration will be

$$\mathbf{x}^j=\mathbf{x}^{j-1}+\mathbf{n}W_n\Delta t. \tag{63}$$

A proper solution is obtained when W_n goes to zero and the interface reaches its steady state position while the governing equations are satisfied in their respective domains. The existence of one and only one solution and the convergence of the iteration procedure to that one solution cannot be assured for nonlinear problems like the present one. However, in several cases different initial conditions were supplied for the same process parameters, or previous solutions were disturbed, and in every case the convergence occurred to the same final solution. Therefore, it appears that the system of finite-difference equations and the differential equations indeed have one and only one solution at least for the range of parameters used here, $0 \leqslant Re \leqslant 50$, $0 \leqslant Gr \leqslant 10^6$, and $Pr = 0{\cdot}02$.

7. RESULTS

To demonstrate the accuracy of the model in computing solid–liquid interface positions it is desirable to compare the results to existing solutions. For the case of finite latent heat no such exact solutions are known. However, an exact solution is available for the case of no latent heat, $S = 0$, with slug flow and no free convection in the liquid, $Gr = 0$, and constant and equal material properties in the solid and liquid region, i.e. $\mu = 1$ and $P = RePr$, corresponding to the problem of linear heat conduction in a moving single phase body.

Figure 2 compares the exact interface with the numerical solutions of the present model using 9×9 and 18×18 nodal networks. The results are very good regarding the overall pool shape, with some difference in the curvature of the interface in the upper parts of the pool. Figure 3 shows the coordinate lines of the mapped plane plotted onto the physical plane, indicating that the solid region has only very few node points in the corner, $y \to 1$. Therefore, some angular coordinate stretching was applied for the solid region by adding an additional transformation in the mapped plane (see Appendix A). The resulting interface of Fig. 4 is indeed even closer to the exact solution.

Next the case of infinite latent heat but with slug flow in the liquid was considered, disregarding free convection effects, i.e. $Gr = 0$. In this case one can solve the solid and liquid energy equations together with the interface boundary conditions, omitting the vorticity and stream function equations. This corresponds to the case investigated by other authors, using single-region models [13–15]. The present two-region model avoids the inaccuracies of one-region models in particular close to the interface [9], however, at this time it is restricted to constant temperature boundary conditions and to shallow pools. Since the previous single region models used different process parameters and boundary conditions a direct comparison cannot be made.

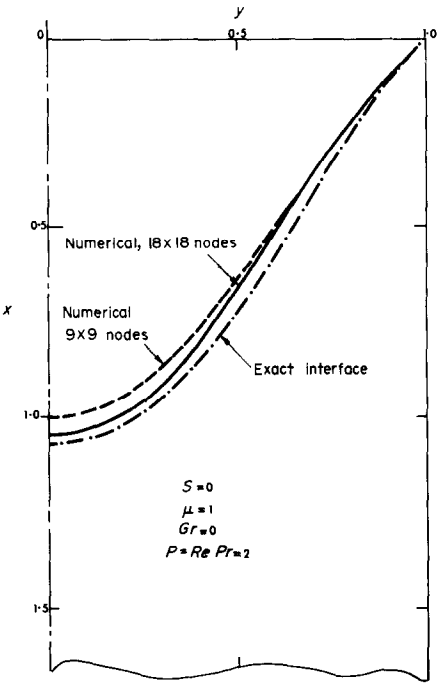

FIG. 2. Solid–liquid interface for case of no latent heat and slug flow in the liquid.

For this slug flow case the following non-dimensional parameters enter the problem:

$$P, \quad RePr, \quad S, \quad \mu$$

where $RePr$ is used for the liquid region Peclet number to distinguish it from P for the solid region. The present model uses different temperature scales for the solid and liquid regions, [see equation (15)]. To relate solid and liquid region temperatures, a common reference base is desired and a new dimensionless temperature is defined relating all temperature differences to $(T_s - T_{amb})$:

$$\tau = \frac{T - T_{amb}}{T_s - T_{amb}}. \tag{64}$$

This scale assigns $\tau = 0$ as ambient temperature and $\tau = 1{\cdot}0$ as the solidification temperature.

The cooling rate of the process can then be characterized by the temperature difference

$$\Delta\tau_c = \frac{T_s - T_0}{T_s - T_{amb}} = 1 - \tau_0. \tag{65}$$

The Stefan number can be expressed as

$$S = \frac{S^*}{\Delta\tau_c} \tag{66}$$

where the "ambient Stefan number"

$$S^* = \frac{\Delta H}{c_S(T_s - T_{amb})} \tag{67}$$

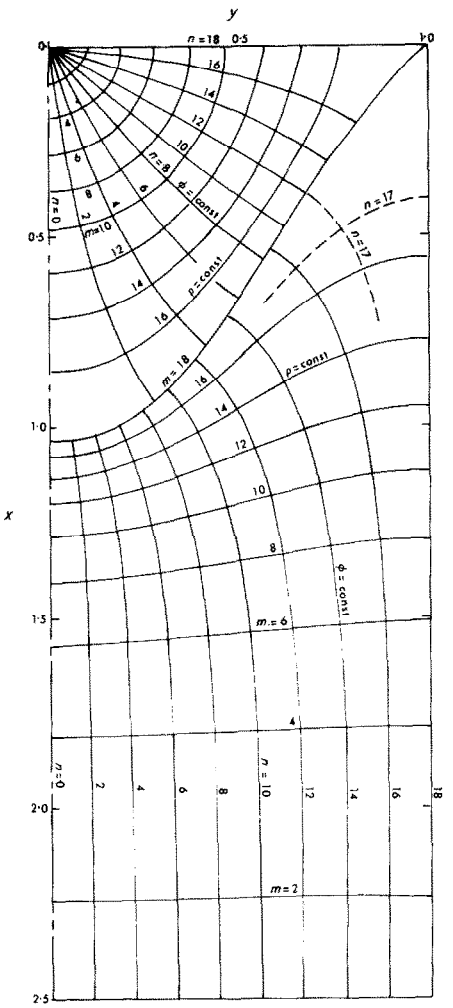

FIG. 3. Coordinate line correspondence between mapped plane and physical plane.

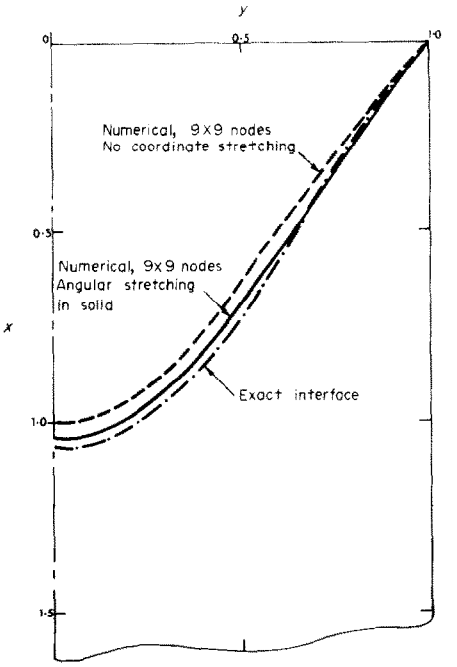

FIG. 4. Solid–liquid interface for case of no latent heat and slug flow in the liquid, with angular coordinate stretching.

is strictly material property dependent and varies for the most common metals from 0·27 for iron to 1·1 for tin, with copper having a value of 0·42. This rearrangement shows S to characterize the latent heat of the material and the process cooling rate.

Finally the conductivity–temperature ratio can be expressed as

$$\mu = \frac{k_L \Delta\tau_{SH}}{k_S \Delta\tau_c} \tag{68}$$

i.e. it is affected by material properties, feed metal superheat and cooling rate.

Thus, the three independent process variables, withdrawal speed U_w, superheat $(T_f - T_s)$, and the outside cooling rate characterized by $(T_s - T_0)$ enter as non-dimensional parameters P, $\Delta\tau_{SH}$, and $\Delta\tau_c$. The material properties enter through S^* for the latent heat and through the conductivity and diffusivity ratios k_L/k_S and α_L/α_S, where $k_L/k_S \approx \alpha_L/\alpha_S$ for most metals of interest.

The effect of latent heat on the interface position is shown in Fig. 5. At higher levels of latent heat the liquid pools get deeper, providing more surface area for the increased energy flow out of the interface. At the same time the temperature gradients on the solid side of the interface get steeper as indicated in Fig. 6, where with increasing S the discontinuity in gradients at the interface ($\tau = 1$) becomes more pronounced.

The liquid pools of Fig. 5 could also be considered as those for constant latent heat S^* with varying cooling rate and feed metal superheat, higher S meaning lower $\Delta\tau_c$ and lower superheat $\Delta\tau_{SH}$ for constant μ.

The effects of changes in withdrawal velocity (P) and cooling rate ($\Delta\tau_c$) for a material like copper and at constant feed metal superheat are shown in Fig. 7. The pool depth increases by about the same amount as P is doubled or as $\Delta\tau_c$ is halved. However, with higher withdrawal velocity corresponding to an increased energy flow across the interface, a longer, more curved interface is obtained.

In Fig. 8 the complete temperature field for a typical continuous casting process is presented for later reference. Both, the solid ($\tau < 1$) and the liquid region ($\tau > 1$) are shown.

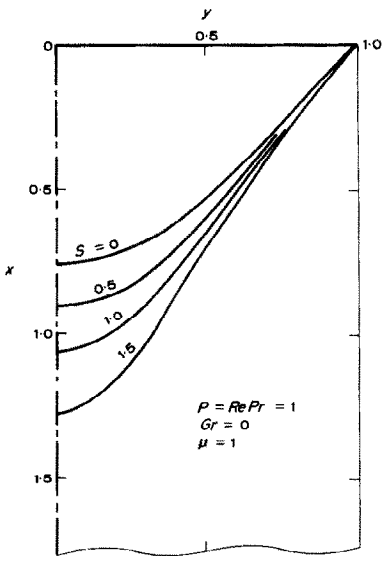

FIG. 5. Solid–liquid interfaces at various levels of latent heat, with slug flow in the liquid.

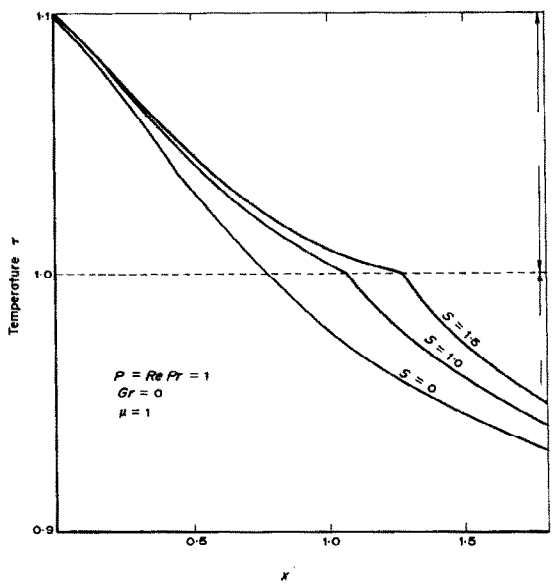

FIG. 6. Axial temperature profiles at various levels of latent heat, with slug flow in the liquid.

The most general form of the model will now be considered, including natural convection effects in the liquid region. The following runs used the complete model with an 18×18 nodal network and material properties close to those of copper ($S^* = 0{\cdot}4$, $k_L/k_S = \alpha_L/\alpha_S = 0{\cdot}5$ and $Pr = 0{\cdot}02$). The process operating conditions are $P = 0{\cdot}5$, $\Delta\tau_{SH} = 0{\cdot}1$ and $\Delta\tau_c = 0{\cdot}1$,

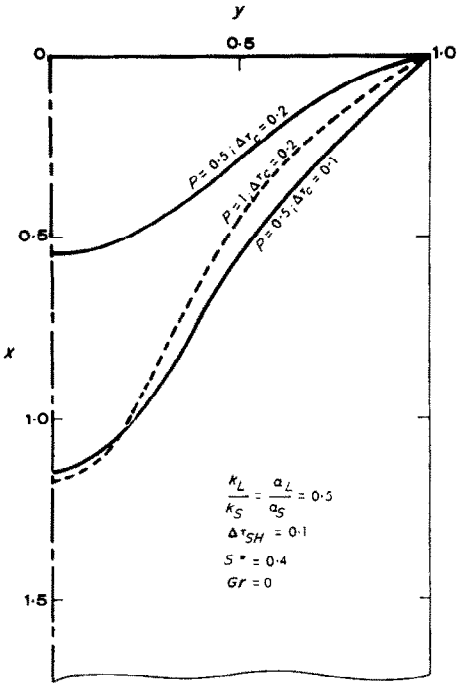

FIG. 7. Effect of increased withdrawal velocity and of decreased cooling rate on the interface position, with slug flow in the liquid.

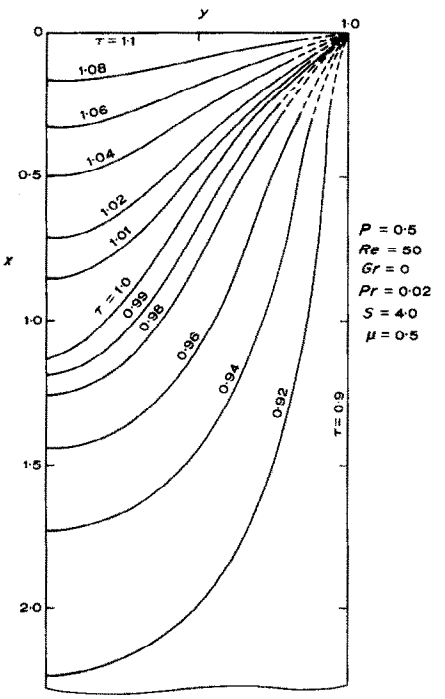

FIG. 8. Solid and liquid temperature field, with slug flow in the liquid.

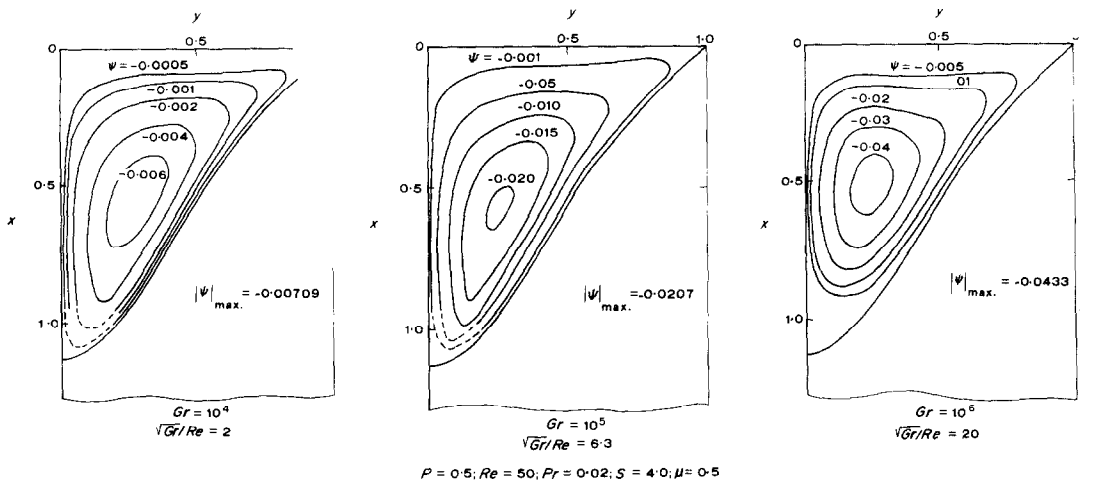

FIG. 9. Natural convection streamlines for combined forced and natural convection in the liquid.

resulting in $Re = 50$, $S = 4{\cdot}0$ and $\mu = 0{\cdot}5$. The Grashof numbers considered for various levels of natural convection* are 0, 10^4, 10^5 and 10^6. Figure 9 shows the natural convection stream function field for various Grashof numbers. In particular at $Gr = 10^6$ a significant amount of natural convection is seen to be present. The total volume flow due to natural convection per unit depth of the slab is

$$Q_{NC} = U_0 Y_0 |\psi|_{\max} \tag{69}$$

or as fraction of the forced flow

$$\frac{Q_{NC}}{Q_{FF}} = \frac{U_0}{U_w}|\psi|_{\max} = \frac{\sqrt{(Gr)}}{Re}|\psi|_{\max}. \tag{70}$$

Thus, at $Gr = 10^4$ the volume flow due to natural convection amounts to only 1·4 per cent of the forced flow, however, at $Gr = 10^6$ it represents 87 per cent of the forced flow. While the forced flow is uniformly distributed over the range $0 < y < 1$, all natural convection flow must pass between the point of $|\psi|_{\max}$ and the interface, as well as between that point and the centerline. Accordingly, the natural convection peak velocities at $Gr = 10^6$ can well exceed the forced flow velocity U_w. Indeed, for the natural convection flow fields of Fig. 9 one finds for $Gr = 10^6$ at about one half the depth of the pool and close to the interface a maximum velocity tangential to the interface of $v_t = 0{\cdot}47$. In terms of the forced flow velocity this is

$$\frac{V_t}{U_w} = \frac{U_0}{U_w}v_t = \frac{\sqrt{(Gr)}}{Re}v_t = 20 \times 0{\cdot}47 = 9{\cdot}4$$

i.e. in this case the peak natural convection velocity is almost 10-times larger than the withdrawal speed! For the case $Gr = 10^4$ the peak velocity $v_t = 0{\cdot}064$ is about an order smaller resulting in a value of $V_t/U_w = 0{\cdot}128$ only.

Defining a stream function Φ for the combined flow field.

$$\frac{U}{U_w} = \frac{\partial \Phi}{\partial y}; \quad \frac{V}{U_w} = -\frac{\partial \Phi}{\partial y} \tag{71}$$

this stream function can be expressed in terms of ψ as

$$\Phi = y + \frac{\sqrt{(Gr)}}{Re}\psi. \tag{72}$$

Figure 10 shows the stream lines of the combined forced and natural convection flow field for several Grashof numbers. While the effects of natural convection are small at $Gr = 10^4[\sqrt{(Gr)}/Re = 2]$ they clearly dominate at $Gr = 10^6[\sqrt{(Gr)}/Re = 20]$ with backward flow at the center line.

Figure 11 shows the liquid region temperature field for $Gr = 10^4$ and $Gr = 10^6$. The convective terms in the energy equation are multiplied by the Prandtl number and, thus, the effects of the flow field on the temperature field will be less pronounced for small Prandtl number fluids. At $Gr = 10^4$ the temperature field was virtually identical to the slug flow case $Gr = 0$, of Fig. 8. And even at $Gr = 10^6$, with drastically changed flow field, the effect on the temperature field was not very severe. In the top region of the pool, the isotherm positions are only slightly different from those for $Gr = 0$. In the bottom region of the pool the isotherms are "swept" upward by the backward flow. The temperature gradients in this part of the pool are less than half of those without natural convection.

*For copper, with the superheat given above and for a characteristic dimension $Y_0 = 1$ cm the Grashof number would be about 3×10^5.

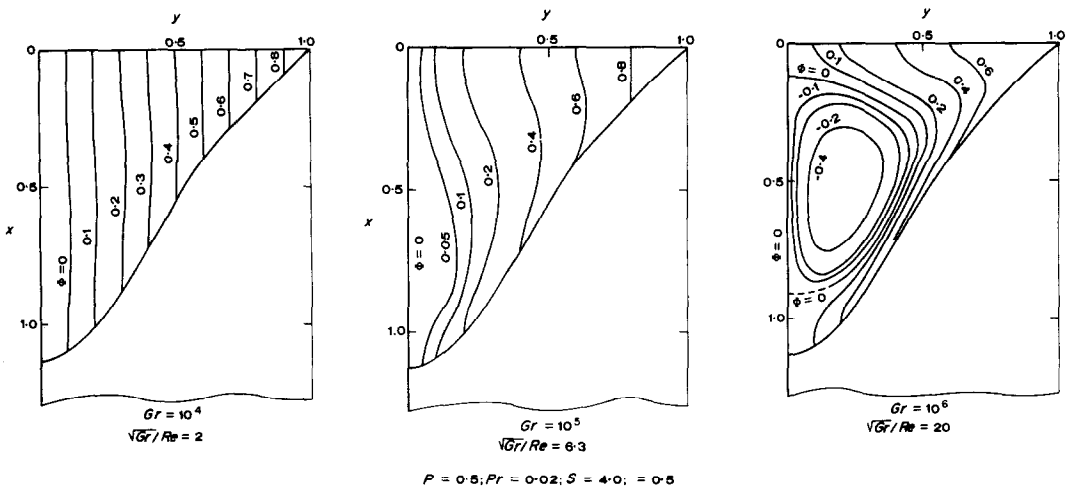

FIG. 10. Streamlines of the combined forced and natural convection flow field.

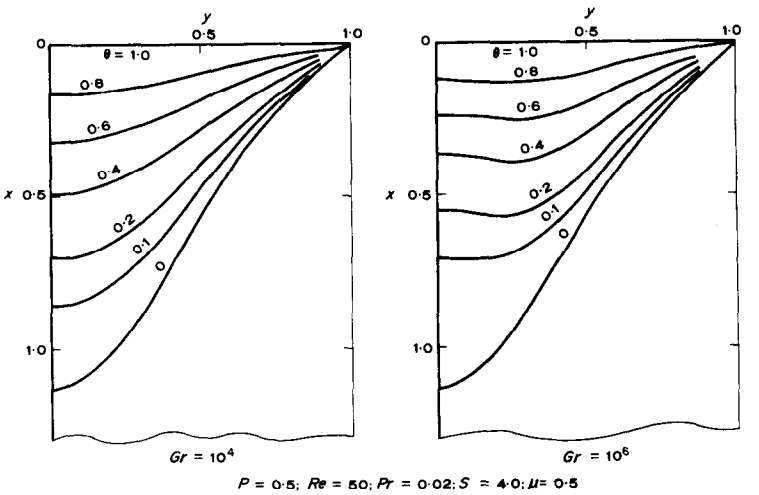

FIG. 11. Temperature field with forced and natural convection in the liquid.

The solid–liquid interface position with (33) is affected by

$$-\frac{\partial\theta}{\partial n}+\mu\frac{\partial\Theta}{\partial n}.$$

In top regions of the pool the liquid side gradient $\partial\Theta/\partial n$ changes only very little with free convection, and at the bottom the liquid side term $\mu|\partial\Theta/\partial n|$ is very small compared to the solid side term $|\partial\Theta/\partial n|$. The changes in the liquid temperature field due to natural convection should, therefore, not affect the interface position much. In the present runs they were well within plotting accuracy, and thus, insignificant. For pools deeper than the present runs the natural convection field could conceivably be stronger; however, the temperature gradients towards the bottom would then generally be even smaller. The negligible effect of the natural convection field on the interface corresponds to the expectations of Section 2. However, the flow field in itself remains of interest, due to its potential effects on the solidification process and on the ultimate structure of the casting.

8. IMPLICATIONS

The general analysis developed here offers more accurate results than can be obtained with single region models of the temperature and flow fields in continuous casting processes. The model is the first one known to include natural convection effects in the liquid pool of a continuous casting process. In the present form of the model the investigations generally had to be restricted to shallow pools, $x_p < 1{\cdot}3$, and to a uniform forced flow $Re < 50$.

The results show that for liquid metals even in such shallow pools natural convection flows of significant

magnitude can arise, and that the peak velocities of the natural flow field, relative to the motion of the casting, can even exceed the forced flow withdrawal speed. Depending on the type of dendrite structure and on the strength of the dendrite tips and arms this can have significant effects on the ultimate cast structure, for instance due to arms being broken off, and being swept downward into the bottom of the pool.

Results further show that the effect of the natural convection flow field on liquid region temperatures remains relatively minor in top regions of the pool. However, it does further enhance the formation of an almost isothermal region at the bottom of the pool, in particular as the pool depth increases.

Through control of the governing nondimensional parameters, and in particular through the superheat, $\Delta\tau_{SH}$, and the Grashof number, Gr, one can affect the strength of the natural convection flow field to obtain a quiet uniform forced flow, or a strongly stirred pool, even with upward flow at the center line, whichever is desired.

Within the range of the parameters investigated, it was found that even for a strong natural convection field there was almost no effect on the solid–liquid interface position. It is expected that this result would also hold for some deeper pools and higher Reynolds numbers. Thus, for known or well estimated pool shapes, natural convection effects may often be studied by solving the liquid region equation only, with assumed interface position, thus avoiding the expensive iterative procedure of recomputing pool shapes.

Acknowledgement—This research was sponsored by the Casting Laboratory of Chase Brass and Copper Company, subsidiary of Kennecott Copper Corporation. The support of the Laboratory is gratefully acknowledged. The authors thank Mrs. Nancy C. Hetrick for her diligent help during the preparation and running of the computer program.

REFERENCES

1. H. S. Carslaw and J. C. Jaeger, *Conduction of Heat in Solids*, 2nd Edn. Oxford University Press, Oxford (1959).
2. A. L. London and R. A. Seban, Rate of ice formation, *Trans. Am. Soc. Mech. Engrs* **64**, 771 (1943).
3. T. R. Goodman, The heat balance integral and its application to problems involving a change of phase, *Trans. Am. Soc. Mech. Engrs* **80**, 335 (1958).
4. F. Megerlin, Geometrische eindimensionale Wärmeleitung beim Schmelzen und Erstarren, *Forsch. Geb. IngWes.* **34**, 40 (1968).
5. Y. A. Samoilovich, Application of the Biot variational method for solution of the Stefan problem, *High Temperature* **4**, 771 (1966).
6. C. M. Adams, Thermal considerations in freezing, *Liquid Metals and Solidification*. ASM, Cleveland (1958).
7. G. M. Dusinberre, *Numerical Analysis of Heat Flow*. McGraw-Hill, New York (1949).
8. N. R. Eyres, D. R. Hartree, J. Ingham, R. Jackson, R. J. Sargant and J. B. Wagstaff, The calculation of variable heat flow in solids, *Phil. Trans. R. Soc.* **240**, Ser. A. 1 (1947).
9. W. D. Murray and F. Landis, Numerical and machine solutions of transient heat conduction problems involving melting or freezing, *Trans. Am. Soc. Mech. Engrs* **81**, 106 (1959).
10. A. Lazaridis, A numerical solution of the multidimensional solidification of melting problem, *Int. J. Heat Mass Transfer* **13**, 1459 (1970).
11. A. W. D. Hills, A generalized integral profile method for the analysis of unidirectional heat flow during solidification, *Trans. TMS–AIME* **245**, 1471 (1969)
12. A. I. Veynik, *Theory of Special Casting Methods*. Am. Soc. Mech. Engrs, New York (1958).
13. P. G. Kroeger, A heat transfer analysis of solidification of pure metals in continuous casting process, in *Heat Transfer 1970*, Proc. 4th Int. Heat Transfer Conference, Vol. 1, Cu 2.7. Paris (1970).
14. H. Klein, Die physikalischen und mathematischen Grundlagen zur Berechnung der Abkuehlung des Stranges beim Stranggusz von Metallen mit Hilfe von Differenzengleichungen, *Giesserei*, Heft 10 (1953).
15. D. J. P. Adenis, K. H. Coats and D. V. Ragone, An analysis of the direct-chill-casting process by numerical methods, *J. Inst. Metals* **91**, 395 (1962).
16. J. Szekely and V. Stanek, On the heat transfer and liquid mixing in the continuous casting of steel, *Met. Trans.* **1**, 119 (1970).
17. R. Mehrabian, M. Kean and M. C. Flemings, Interdendritic fluid flow and macrosegregation; influence of gravity, *Met. Trans.* **1**, 1209 (1970).
18. P. G. Kroeger, The free surface problem of flow and temperature fields during solidification in a two-dimensional moving system, Ph. D. Thesis, Case Western Reserve University (1972).
19. S. Ostrach, Laminar flows with body forces, article F of theory of laminar flows, edited by F. K. Moore, *High Speed Aerodynamics and Jet Propulsion*, Vol. IV. Princeton University Press, Princeton, N. J. (1964).
20. J. R. Lloyd and E. M. Sparrow, Combined forced and free convection flow on vertical surfaces, *Int. J. Heat Mass Transfer* **13**, 434 (1970).
21. D. Gaier, Konstruktive Methoden der konformen Abbildugen, in *Springer Tracts in Natural Philosophy*. Springer, Berlin (1964).
22. H. Wittich, Konforme Abbildung einfach Zasammenhaengender Gebiete, *Z. Angew. Math. Mech.* **25/27**, 131 (1947).
23. L. Collatz, *The Numerical Treatment of Differential Equations*, 3rd Edn. Springer, Berlin (1966).
24. G. E. Forsythe, W. R. Wasow, *Finite Difference Methods for Partial Differential Equations*. John Wiley, New York (1960).
25. I. S. Sokolinikoff, *Tensor Analysis*, 2nd Edn. John Wiley, New York (1964).
26. H. W. Emmons, Critique of numerical modeling of fluid-mechanics phenomena, in *Annual Review of Fluid Mechanics*, Vol. 2, edited by M. Dyke, W. G. Vincenti and S. V. Wehausen. Annual Review, Palo Alto, Ca. (1970).
27. S. I. Cheng, Numerical integration of Navier–Stokes equations. *AIAA Jl* **8**, 2115 (1970).
28. G. D. Mallinson and G. deVahl Davis, The method of the false transient: application to fluid mechanics, The University of New South Wales, School of Mechanical and Industrial Engineering, Report No. 1971/FMT/2, Kensington, New South Wales (1971).

APPENDIX A

Conformal Mapping of the Solid and the Liquid Region

To employ the above procedure the mapped domains and a corresponding sequence of mappings must be selected. The selected sequence of mappings is shown schematically in Fig. A1:

For the liquid region a logical choice is to map the liquid pool plus its mirror image in $x < 0$ into the unit circle.

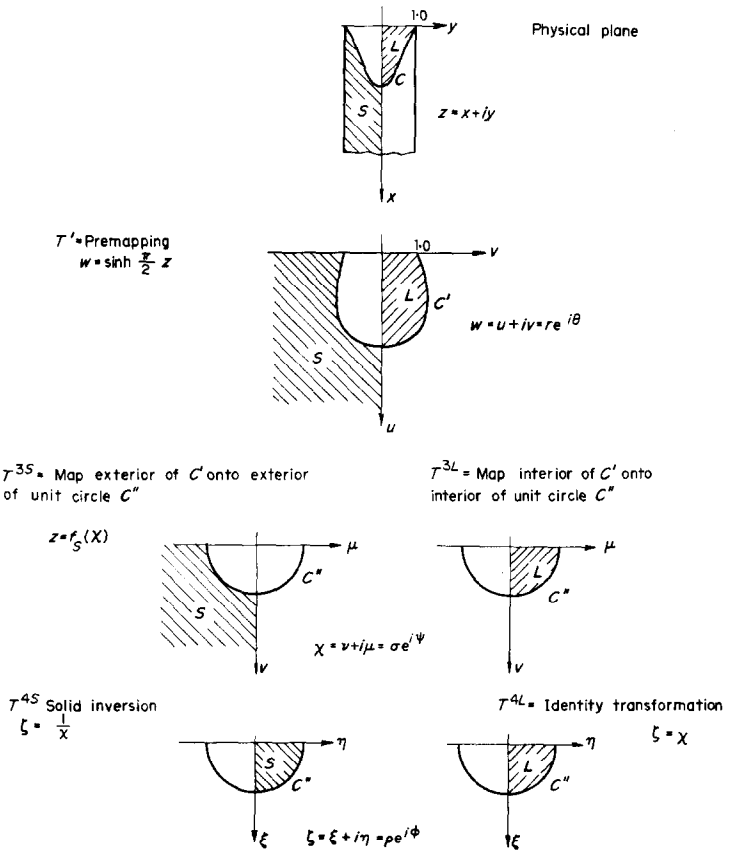

FIG. A1. Sequence of mappings.

A procedure to transform the solid region into a regular domain is not obvious, and several possibilities exist. It was decided to proceed here as follows: The complete slab of liquid and solid domain $x > 0$, $-1 < y < +1$, can be transformed into the half plane $u > 0$ by the conformal mapping

$$w = \sinh\frac{\pi}{2}z. \tag{A1}$$

The solid–liquid interface C is mapped here into the contour C'. Thereafter, applying a general conformal mapping which maps the exterior of C' and its mirror image in $u < 0$ onto the exterior of the unit circle C'', one obtains a regular domain for the solid, including the point at infinity. To avoid the numerical difficulty of satisfying boundary conditions at infinity one can apply the inversion

$$\zeta = \frac{1}{\chi}, \tag{A2}$$

mapping the solid conformally into the interior of the unit circle. This latter transformation includes a reflection about the ν-axis, and the first quadrant of the unit circle in the mapped plane will now correspond to the negative half of the solid domain in the physical plane.

Once this sequence of mappings has been selected for the solid region, it is convenient, but by no means necessary, to apply the pre-mapping of equation (A1) to the liquid region as well. Similarly, for convenience in notation an identity transformation T^4, $\zeta = \chi$ has been added for the liquid, corresponding to the solid inversion equation (A2).

For the transformation of the governing equations an overall transformation matrix between the physical plane and the mapped plane will be required. It will be convenient to include into this matrix a transformation from cartesian to polar coordinates in the w-plane. Furthermore, if desired, one could add a coordinate stretching transformation in the mapped plane to obtain finer node spacing in the region of steep gradient.

A method must be devised for the transform T^3, conformally mapping, for the solid, the exterior of the arbitrary

contour C' onto the exterior of the unit circle, and for the liquid, the interior of C' onto the interior of the unit circle. Several methods are available for this purpose [18] and Theodorsen's integral equation appeared most desirable for the problem at hand.

In using this method the conformal mapping between points of the w plane and the χ plane $w = f(\chi)$ is expressed in the form

$$F(\chi) = \ln \frac{f(\chi)}{\chi} = U(\sigma, \psi) + iV(\sigma, \psi) \tag{A3}$$

where U and V are the radius ratio function

$$U(\sigma, \Psi) = \ln \frac{r[\Theta(\sigma, \psi)]}{\sigma} \tag{A4}$$

and its harmonic conjugate, the angular distortion function

$$V(\sigma, \Psi) = \Theta(\sigma, \Psi) - \Psi; \quad V(\sigma, 0) = 0. \tag{A5}$$

With the curve C' in the w plane expressed in the form $r(\Theta)$ Theodorsen's integral equation describes the conformal mapping between the unit circle C'' in the χ plane and the curve C' in the w-plane in terms of the function $\Theta(\Psi)$:

$$\Theta(\Psi) = \pm \frac{1}{2\pi}(P) \int_0^{2\pi} \ln r[\Theta(\tau)] \cot \frac{\Psi - \tau}{2} d\tau. \tag{A6}$$

The plus sign applies for the interior to interior mapping, and the minus sign for the exterior to exterior case. The integral is to be taken as a Cauchy principal value.

The solution to the above integral equation determines, in principle, the desired conformal mappings by providing the radius ratio function and the angular distortion function on the unit circle. The U and V in the interior of the unit circle then follow directly from Poisson's integral formula:

$$F(\sigma, \Psi) = \pm \frac{1}{2\pi} \int_0^{2\pi} F(e^{i\tau}) \frac{1 - \sigma^2}{1 - 2\sigma \cos(\tau - \Psi) + \sigma^2} d\tau \tag{A7}$$

where F represents either U or V. Again, the plus sign applies for the interior to interior case of the liquid region and the minus sign for the exterior case of the solid.

For domains with arbitrary boundaries closed form solutions of (A6) are usually not available and the nonlinear, singular integral equation must be solved by numerical methods. Several methods are available to solve this integral equation. A comparison by Gaier [21] showed Wittich's method [22, 23] to give the best results. The application of this method to the present problem is outlined in detail in [18]. Using a truncated Fourier series to approximate $\ln[r(\Theta)]$ the solution to (A6) at $2N$ discrete points on the unit circle

$$\Psi_k = q_k; \quad q = \frac{\pi}{N}; \quad -N + 1 \leqslant k \leqslant N \tag{A8}$$

is obtained by iterative application of the $2N$ nonlinear simultaneous equations:

$$\Theta^{i+1}(\Psi_k) - = kq + \frac{1}{N} \sum_{\substack{\mu = -N+1 \\ (k-\mu \text{ odd})}}^{N} \ln r[\Theta^i(t\mu)] \cot \frac{k - \mu}{2} q. \tag{A9}$$

For the present special case of quarter circle symmetry, (A9) can be reduced to

$$0 \leqslant \mu \leqslant n = N/2 \ (N \text{ even}):$$

$$\Theta^{i+1}(\phi_k) = kq \pm \frac{1}{n}(T_1 + T_2 + T_3) \tag{A10}$$

with

$$T_1 = \begin{cases} 0 & ; \ k \text{ even} \\ \ln r(0) \cot kq; & k \text{ odd} \end{cases} \tag{A10a}$$

$$T_2 = \sum_{\substack{\mu = 1 \\ (\mu \text{ odd})}}^{n-k-1} \ln r[\Theta^i(t_{k+\mu})] [\cot(2k + \mu)q - \cot \mu q] + \sum_{\substack{\mu = 1 \\ (\mu \text{ odd})}}^{k-1} \ln r[\Theta^i(t_{k-\mu})] [\cot(2k - \mu)q + \cot \mu q] \tag{A10b}$$

$$T_3 = \begin{cases} 0 & ; \ k - n \text{ even} \\ -\ln r\left(\frac{\pi}{2}\right) \tan kq; & k - n \text{ odd}. \end{cases} \tag{A10c}$$

The brackets of (A10b) can be expressed in alternate, algebraically more compact forms; however, for numerical computations the above form was found to be most convenient.

In the present problem the derivative of $\ln r(\Theta)$ with respect to Θ will be discontinuous at $\Theta = \pm \pi/2$. The truncation error of (A9) is then $0\,(1/n)$ [21]. However, since n grows only linearly as the discretization is refined one can select n sufficiently large to get very accurate solutions as evidenced by the trial mappings of [18], Appendix F. Further considerations regarding the existence of solutions and the convergence of the sequence (A10) are also given in [18]. The evaluation of U and V in the interior or exterior of the unit circle by numerical integration of (A7) is straightforward, except that close to the unit circle the Poisson kernel gets very peaked and special care must be taken to obtain results of sufficient accuracy. Several ways to achieve this are discussed in [18]. Here a separate integration over the region of peaked kernels with a very fine nodal spacing, and with a coarser spacing over the remainder of the integration domain provided sufficient accuracy.

To transform the governing equations of the physical plane into the mapped plane the transformation must be given, connecting the (x, y) coordinate system of the physical plane with the $\rho, \phi)$ coordinate system of the mapped plane:

$$T = \begin{pmatrix} \frac{\partial x}{\partial \rho} & \frac{\partial x}{\partial \phi} \\ \frac{\partial y}{\partial \rho} & \frac{\partial y}{\partial \phi} \end{pmatrix}. \tag{A11}$$

The scale factors follow from the matrix coefficients as

$$h_1 = \sqrt{\left[\left(\frac{\partial x}{\partial \rho}\right)^2 + \left(\frac{\partial y}{\partial \rho}\right)^2\right]} \tag{A12}$$

$$h_2 = \sqrt{\left[\left(\frac{\partial x}{\partial \phi}\right)^2 + \left(\frac{\partial y}{\partial \phi}\right)^2\right]}. \tag{A13}$$

To compute the matrix coefficients and scale factor one must have in addition to the mapping functions U and V also their derivatives. In the interior or exterior of the unit circle these were obtained by differentiating (A7). On the unit circle they were computed from a centered second order finite difference equation. Possible refinements of this procedure are discussed in [18].

The pre-mapping transform T^1 induced some limitations in the method. This transformation is used to extend the solid domain over the complete exterior of the interface, C', in Fig. A1. It has singular points at $z = \pm i$, where the right angle between the y axis and the slab surface $y = \pm 1$ is mapped into an angle of 180°. For deep pools the interface tangent in the w plane will at this point intersect the v-axis at a very shallow angle, causing convergence problems in the numerical solution of (A10).

For deeper pools a different mapping procedure would have to be used for the solid or the relatively simple governing equation of the solid (24) could be solved directly in the physical domain using a noneven nodal spacing [24]. For the liquid region this limitation does not apply, T^1 is only used there for convenience and could be omitted permitting the mapping of a great variety of liquid pools.

For the present work shallow pools were of primary interest and this limitation was therefore not essential.

SOLUTION DU PROBLEME BIDIMENSIONNEL DE LA SOLIDIFICATION INCLUANT LES EFFETS DE CONVECTION DANS LA REGION LIQUIDE

Résumé—On considère les champs de température et de vitesse durant la solidification d'un métal pur dans une plaque mobile pour application au processus de coulée continue. L'analyse considère la convection naturelle dans le noyau liquide.

De forts courants de convection naturelle se produisent à des nombres de Grashof de l'ordre de 10^5–10^6. Néanmoins pour les domaines de paramètres étudiés la convection naturelle a un effet négligeable sur la position de l'interface solide–liquide.

On présente des aspects qualitatifs nombreux sur l'écoulement mixte dans le noyau liquide. Même pour une convection naturelle très intense, l'effet du champ de vitesse sur le champ de température reste relativement réduit, sa tendance principale est de favoriser la formation d'une région isotherme à la base du noyau.

DIE LÖSUNG EINES ZWEIDIMENSIONALEN ERSTARRUNGSPROBLEMS UNTER BERÜCKSICHTIGUNG DER KONVEKTION IN DER FLÜSSIGKEIT

Zusammenfassung—Zur Simulation eines kontinuierlichen Gießvorgangs wird das Temperatur- und Strömungsfeld während der Erstarrung eines reinen Metalles in einen beweglichen Stab betrachtet.

Bei Grashof-Zahlen von 10^5 bis 10^6 liegt eine starke freie Konvektion vor, die im untersuchten Bereich allerdings nur einen unwesentlichen Einfluß auf die Lage der Erstarrungs-Phasengrenzfläche hatte.

Die Überlagerung von erzwungener und freier Konvektion wird unter qualitativen Gesichtspunkten dargelegt. Selbst bei sehr starker freier Konvektion übt das Strömungsfeld nur einen relativ geringfügigen Einfluß auf das Temperaturfeld aus, wobei die Tendenz zur Bildung einer nahezu isothermen Flüssigkeitsregion in der Nähe der Erstarrungs-Phasengrenzfläche verstärkt wird.

РЕШЕНИЕ ДВУМЕРНОЙ ЗАДАЧИ О ЗАМЕРЗАНИИ ПРИ НАЛИЧИИ КОНВЕКЦИИ В ЖИДКОСТИ

Аннотация — С целью интенсификации непрерывного процесса литья рассматривается поле температур и скоростей при затвердевании чистого металла в движущейся плите. В этом случае учитывается влияние естественной конвекции в резервуаре с жидкостью. В диапазоне чисел Грасгофа $10^5 = 10^6$ имеют место сильные потоки при естественной конвекции. Однако, в исследуемом диапазоне параметров естественная конвекция незначительно влияет на расположение поверхности раздела: твердое тело–жидкость.

Приводятся различные качественные аспекты поля скоростей при вынужденной и естественной конвекции в резервуаре с жидкостью.

Даже при весьма интенсивной естественной конвекции поле скоростей незначительно влияет на поле температур и, в основном, способствует образованию почти изотермической области в нижней части резервуара.